JOURNAL OF Materials CHEMISTRY

Template-assisted self-assembly of macro–micro bifunctional porous materials

Guangshan Zhu,[a,b] Shilun Qiu,*[b] Feifei Gao,[b] Dongsheng Li,[b] Yafeng Li,[b] Runwei Wang,[b] Bo Gao,[b] Binsong Li,[b] Yanghong Guo,[b] Ruren Xu,[b] Zheng Liu[a] and Osamu Terasaki*[a]

[a]*CREST, Japan Science and Technology Corporation and Department of Physics, Tohoku University, Sendai 980-8578, Japan. E-mail: terasaki@msp.phys.tohoku.ac.jp; Fax: (+81)-22-217-6474*

[b]*Key Laboratory of Inorganic Synthesis and Preparative Chemistry, Jilin University, Changchun 130023, China. E-mail: sqiu@mail.jlu.edu.cn; Fax: (+86)-431-567-1974*

Received 1st November 2000, Accepted 20th February 2001
First published as an Advance Article on the web 3rd April 2001

The preparation of macro–micro bifunctional porous materials has been accomplished by a well-controlled, vacuum-assisted technique. Monodisperse polystyrene latex spheres were ordered into close-packed arrays by slow sedimentation, allowing a high flux of water through the interstices between latex spheres. Zeolite LTA, FAU, LTL, BEA, MFI and Si-MFI nanocrystals, synthesized by hydrothermal procedures, permeated the interstices of latex spheres under the driving force of flowing water. After drying and calcination at 500 °C, both the latex spheres and zeolite structure-directing molecules were removed, followed by the formation of products consisting of both crystalline micropores and periodic, interconnected networks of submicron macropores. XRD, SEM, TEM, IR, TG/DTA, ICP and N_2 adsorption–desorption measurements were performed to monitor the preparation and to characterize the properties of the macro–micro bifunctional porous materials. The materials presented in this paper combine the benefits of both the micropore and macropore regimes. They could potentially improve the efficiency of both separation and catalysis of zeolites.

Introduction

By using various techniques, such as gravity sedimentation,[1–4] vertical deposition,[5] centrifugation[6] and flow of solvent through micromachined channels,[7] monodisperse polystyrene (MPS) or silica colloid spheres can be fabricated into close-packed arrays, which generate submicrometer sphere–air pore systems. Introducing inorganic compounds,[6–11] monomers,[12] metal nanocrystals[13] or carbon[14] into the above air pore systems, followed by extraction, calcination or etching, macroporous materials with inorganic components, polymers, metal or carbon frameworks could be produced. However, the uniform introduction of materials into the air pore system is challenging as the surfaces are not available in the narrow and relatively inaccessible interstitial regions of colloidal spheres and such arrays are relatively fragile and easily disrupted. In order to obtain high quality macroporous materials, efforts must be made to overcome these obstacles. For example, in the preparation of porous Au nanostructures,[13b] the size of the Au nanocrystals must be small enough (15–25 nm) to penetrate the spaces between the latex spheres which have diameters of 270–1000 nm.

It is known that zeolites are crystalline materials with uniform channels in the microporous regime.[15] Some zeolites with various crystal sizes have been synthesized, especially in the nanometer range,[16] for the purposes of creating shorter diffusion paths to improve the efficiency of catalysis and separation. Up to now, narrow size distribution materials as small as 30 nm (LTL),[17] 50 nm (LTA) and 80 nm (FAU)[18] have been synthesized in our lab. Other nanosized zeolites synthesized by hydrothermal techniques are BEA,[19] ZSM-2,[20] SOD[21] and Si-MFI.[22]

Macro–micro or meso–micro porous materials provide bimodal pore systems and combine the benefits of each pore size regime which could potentially improve the efficiency of zeolite catalysis. Recently, Stein *et al.*[23] employed the sol–gel transformation approach to obtain macro–micro porous material with a semi-crystalline zeolite Si-MFI framework. Jacobsen *et al.*[24] employed mesoporous carbon blacks as templates to prepare nanosized zeolites which possess both micro- and meso-porous properties. Huang *et al.*[25] reported the preparation of macro–micro porous materials by the infiltration of nano-silicalite sol into an ordered array of MPS microspheres. However, there is no information on the preparation procedure, macro void periodicity and framework properties in detail. Our aim was to prepare novel three-dimensional highly-ordered macro–micro porous materials with a crystalline zeolite framework. Here, we report in detail on the preparation of highly-ordered three-dimensional macro–micro bifunctional porous materials using zeolite LTA, FAU, LTL, BEA and MFI nanocrystals as building blocks. Products were characterized by powder X-ray diffraction (XRD), scanning electron microscopy (SEM), transmission electron microscopy (TEM) and N_2 adsorption–desorption.

Experimental

Preparation of zeolite nanocrystals

Zeolite nanocrystals were synthesized under hydrothermal conditions in the system $SiO_2 : Al_2O_3 : M_2O : R : H_2O$ (M = Na, K; R represents zeolite structure-directing molecules). Generally, the silica and aluminium sources used were tetraethylorthosilicate (TEOS, 98 wt%, Aldrich) and aluminium isopropoxide (98 wt%, Aldrich), respectively. For the synthesis of LTL, fumed silica (99.8 wt%, 500 $m^2 g^{-1}$, Aldrich) and aluminium hydroxide (AlOH, Sigma) were used. Sodium hydroxide (NaOH, 99.998 wt%), potassium hydroxide (KOH, 99.99 wt%), tetramethylammonium hydroxide (TMAOH,

Table 1 Reaction mixture mol ratio, synthesis conditions, SiO_2/Al_2O_3 product ratios and the average size of zeolite LTA, FAU, LTL, BEA, MFI and Si-MFI nanocrystals

Zeolite code	Reaction mixture mol ratio	Temp./°C	Time/days	SiO_2/Al_2O_3 in products	Average size/nm (SEM)	Ref.
LTA	$3SiO_2 : Al_2O_3 : 3R^a : 0.028NaCl : 276H_2O$	100	14	2.6	60	18
FAU	$3.4SiO_2 : 0.83Al_2O_3 : 4.6R^a : 0.1NaCl : 300H_2O$	100	14	3.6	80	18
LTL	$20SiO_2 : Al_2O_3 : 10K_2O : 400H_2O$	170	0.2	5.3	30	17
BEA	$50SiO_2 : Al_2O_3 : 0.7Na_2O : 25R^b : 750H_2O$	100	7	26.7	50	19
MFI	$25SiO_2 : 0.005Al_2O_3 : 0.1Na_2O : 9R^c : 400H_2O$	100	4	465	90	
Si-MFI	$25SiO_2 : 0.1Na_2O : 9R^c : 480H_2O : 100EtOH$	100	4		90	22

^{a}R = TMAOH. ^{b}R = TEAOH. ^{c}R = TPAOH.

25 wt%, in water), tetraethylammonium hydroxide (TEAOH, 35 wt%, in water), tetrapropylammonium hydroxide (TPAOH, 1 M, in water) and sodium chloride (NaCl, 99 wt%) were used as purchased from Aldrich. Typically, the aluminium source was dissolved in an appropriate amount of ROH (R = TMA, TEA, TPA) solution; when necessary, NaCl or NaOH were also added. After forming a clear solution, TEOS was added dropwise with vigorous stirring, resulting in a homogeneous solution. The final reaction mixture was aged for 2 days before being transferred into a 250 ml polypropylene bottle and placed in an oven at 100 °C for 2–14 days. For the synthesis of LTL, a pretreatment of raw materials was needed,[17] and the final reaction mixture was placed in a sealed stainless steel pressure vessel lined with polytetrafluoroethylene, rotated at 20 rpm and heated at 170 °C for 5 hours. The reaction mixture mol ratio, crystallization temperature and synthesis time for zeolite LTA, FAU, LTL, BEA, MFI and Si-MFI nanocrystals and the SiO_2/Al_2O_3 product ratio are summarized in Table 1.

After crystallization, the resulting products were collected by centrifugation at a speed of 9 krpm for 1 hour. The products were repeatedly dispersed in distilled water using ultrasonication and centrifugation as above to remove the remaining mother liquor until the pH of the dispersion was near to 7. The above solids were then dispersed in water and filtered through a 0.2 μm membrane filter to remove larger particles or impurities. The final products were obtained by centrifugation and drying at 80 °C for 4 hours.

Preparation of macro–micro bifunctional porous materials

The materials and chemicals used were as follows: sulfate-modified monodisperse polystyrene beads (0.46, 1.1, 2.02, 4.6 and 11.9 μm, 0.2 wt%, Aldrich, USA or Nishin EM Co. Japan), 47 mm diameter membrane filter with 0.025 μm pores (Millipore Co., USA) and Tween 20 (Aldrich). The typical preparative procedure used was as follows:

(1) Deposition of MPS beads on the filter. The 8–16 g 0.2 wt% negatively charged MPS latex spheres were diluted in 50 ml deionized water (to which 1 g of non-ionic surfactant, Tween 20, was added to improve the quality of the latex arrays) and then deposited into closely packed arrays by filtering for about 4 hours at 40 kPa. The dilute latex spheres accumulated on the filter surface into densely packed three-dimensional ordered arrays with a thickness of about 20 μm. It was necessary to add more deionized water before accumulation was complete in order to maintain a high flux of water through the latex arrays.

(2) Deposition of zeolite nanocrystals on the filter. 0.01–0.04 g zeolite nanocrystals were dispersed in 500–600 ml deionized water by ultrasonication and then added slowly to the sample prepared above. The deposition of nanosized zeolite particles on the membrane through the deposited latex arrays was carried out at 90 kPa for 24–48 hours.

(3) Drying. After the deposition was complete, the membrane with products was dried at 80 °C for 2 hours and the products were then detached.

(4) Calcination. Both the MPS latex beads and structure-directing molecules or H_2O within the channels of the zeolite were removed by calcination: the temperature was ramped at 1 °C min^{-1} to 350 °C, maintained at this temperature for 3 hours and then increased to 500 °C at a rate of 0.5 °C min^{-1} over 7 hours.

Product analysis

Powder XRD studies were performed on a Philips X'PERT PW3050 diffractometer with CuKα radiation for phase identification, operated at 40 kV and 55 mA. The elemental analysis was conducted on a Perkin-Elmer 2400 elemental analyzer and the inductively coupled plasma (ICP) analysis on a Perkin-Elmer Optima 3300 DV ICP instrument. The particle size distribution of zeolite crystals was determined by field emission-scanning electron microscopy (FE-SEM, JSM-5400F). The morphology, periodicity and crystallinity of the samples was determined by transmission electron microscopy (TEM, JEOL-3010, Cs = 0.6 mm, 300 keV). Infrared spectra were recorded from 400–4000 cm^{-1} on a Nicolet Impact 410 FT-IR spectrometer using KBr pellets. Thermogravimetry (TG) and differential thermal analysis (DTA) were performed on a Perkin-Elmer TGA 7 thermogravimetric analyzer and a DTA-1700 differential thermal analyzer, respectively. The samples were heated under flowing air from 25 to 800 °C at 10 °C min^{-1}. N_2 adsorption–desorption measurements were conducted on an ASAP 2010M porosimeter at 77 K. The total surface areas, pore volumes and pore size distributions were calculated based on Brunauer–Emmett–Teller (BET), *t*-plot and Barrett–Joyner–Halenda (BJH) methods.

Results and discussion

The quality of the template of close-packed MPS latex spheres is one of the most important factors for preparing long-range ordered macro–micro bifunctional porous materials. Fig. 1 shows the SEM image of the top view of the PS beads of 2 μm diameter. This sample exhibits an ordered close-packed arrangement of MPS spheres over a sample area of 20 μm^2, which even extends up to a centimeter area. In principle, the close-packing arrangement could be contributed to face-centered cubic (fcc) (ABCABC…), hexagonal close-packed (hcp) (ABAB…) or randomly stacked arrays. Three dimensional colloidal arrays of latex spheres, such as silica spheres and MPS spheres, can be formed by slow sedimentation or by centrifugation of colloidal dispersions of sphere particles. In our study, a slow sedimentation of MPS latex spheres was employed to grow such highly ordered arrays, which contained large ordered regions of latex spheres and periodic void structures. However, it was problematic to characterize the structure of the sample from SEM images alone, as it was difficult to determine the crystal face from the cross-sectional view. The SEM results suggested that the stacking of this

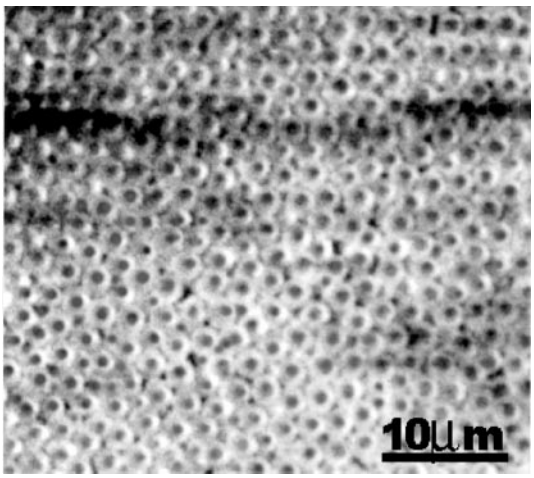

Fig. 1 SEM image of the top view of close-packed MPS latex spheres.

sample between the (111) planes was a random arrangement, in agreement with the result of the stacking of gravity sedimented colloidal crystals,[26] although theoretical calculations have indicated that the fcc structure is slightly more stable.[27]

Fig. 2 shows the SEM image of as-synthesized nanometer sized zeolite FAU crystals. The image indicates that the crystals have a narrow size distribution with diameters of less than 80 nm. The average particle sizes of zeolites LTA, MFI, LTL, BEA and Si-MFI, determined by FE-SEM, are listed in Table 1. The XRD and TEM results measured on the above samples show that all the products were phase pure with more than 98% crystallinity.

In the preparation of macro–micro bifunctional porous materials, the size difference and the mass ratio of MPS latex spheres and zeolite particles are two important parameters as they directly determine whether or not the zeolite particles can penetrate the openings between the latex spheres and permeate all the void structures fabricated by the ordered latex spheres without forming a thick zeolite nanocrystal crust on top of the samples. Sedimentation of MPS latex spheres into hexagonally close-packed arrays can, in principle, result in openings between latex spheres approximately 0.15 times larger than the MPS sphere diameter. To overcome this problem 0.2 μm membrane filters were employed to remove particles or impurities from as-synthesized zeolite products, preventing large particles or impurities blocking the openings between the

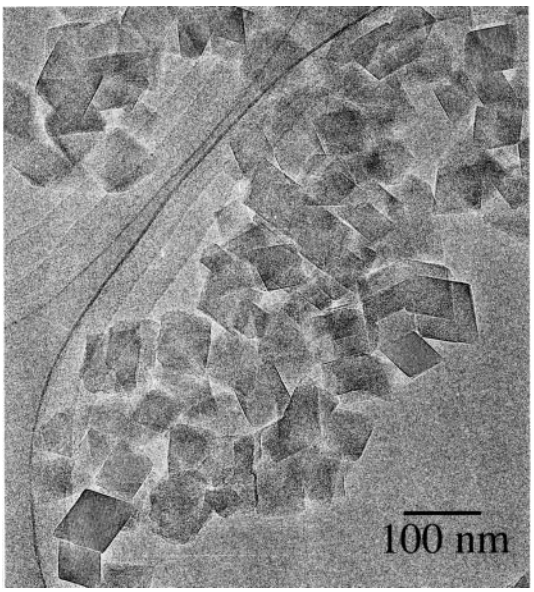

Fig. 2 SEM image of as-synthesized zeolite FAU nanocrystals.

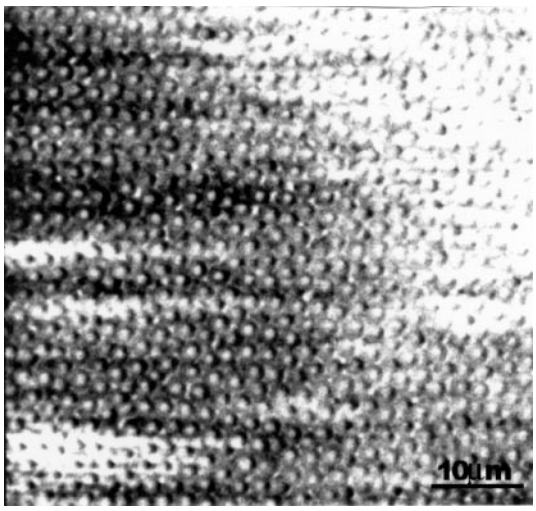

Fig. 3 SEM image (top view) of ordered MPS beads with permeated zeolite FAU nanocrystals.

latex spheres. 2 μm MPS latex spheres were used to sediment slowly into highly ordered arrays, forming periodic void structures with about 309 nm openings allowing zeolite nanocrystals to permeate the voids between latex spheres smoothly. The optimum value of the mass ratio of 2 μm MPS latex spheres to zeolite nanocrystals was about 1, under which conditions zeolite nanocrystals permeated all the voids between the latex spheres without forming a crust on top of the sample.

Fig. 3 presents the SEM image of the top view of ordered MPS latex spheres permeated by zeolite FAU nanocrystals. It indicates that zeolite FAU nanocrystals surround the MPS spheres of the top layer and cover the MPS spheres at some places without the formation of a zeolite crust. The image also

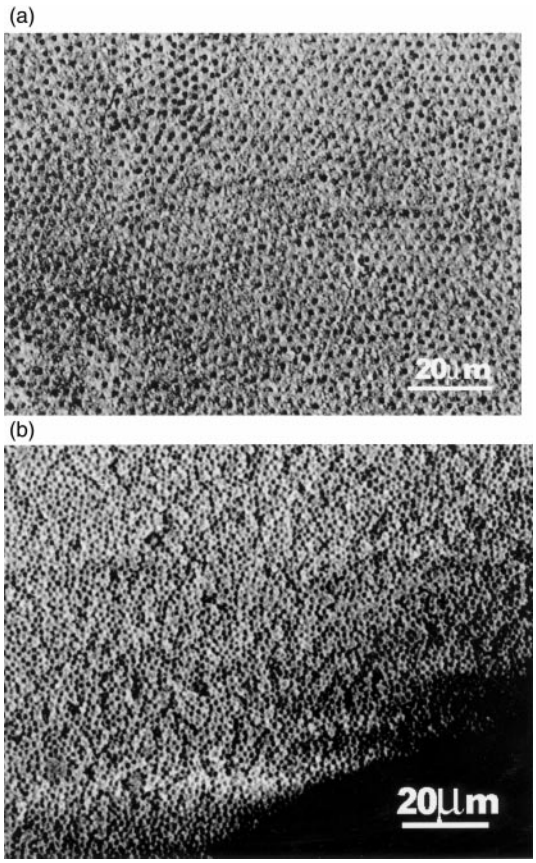

Fig. 4 SEM images of calcined macro–micro bifunctional material using zeolite FAU nanocrystals as building blocks: (a) bottom view and (b) top and side view.

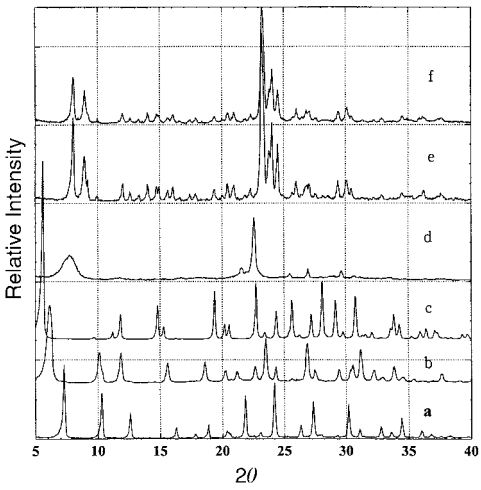

Fig. 5 XRD patterns of calcined macro–micro bifunctional materials as prepared above using zeolite nanocrystals of (a) LTA, (b) FAU, (c) LTL, (d) BEA, (e) MFI and (f) Si-MFI building blocks, respectively.

shows the presence of long-range order and better periodicity of the sample.

Figs. 4a and 4b show the bottom and side view SEM images, respectively, of the calcined material presented in Fig. 3. The macroscopic structure of this sample is a replica of the MPS latex sphere template, exhibiting the arrangement of MPS latex arrays. The void diameter of about 1.7 μm was predetermined by the size of the latex spheres (2 μm), allowing for the shrinkage of the structure after calcination. The bottom of the sample (Fig. 4a) exhibits order over a long length scale. The top and side of the sample (Fig. 4b) have only short-range order.

The removal of the organic templates, both PS latex spheres and zeolite structure-directing molecules (TMAOH, TBAOH or TPAOH) or H_2O by calcination (as described above) creates windows between adjacent voids. Elemental analysis results indicate that the carbon content of the products is in the range of 0.2 to 0.4 wt%, *i.e.* the organic components were almost completely removed by the calcination. Based on the TGA measurements, the amount of inorganic solid remaining after removal of the organic components is from 24 to 39 wt%, corresponding to the weight loss of 76 to 61 wt%. The remaining inorganic components were concerned with zeolite types and the mass ratio of zeolite nanocrystals to MPS latex spheres. For the macro–micro porous material made of zeolite FAU nanocrystals, the weight losses are 23 and 53 wt% with weight loss ranges from 190–250 °C and 250–550 °C, respectively. The former is associated with the removal of H_2O encapsulated in the supercages of zeolite FAU nanocrystals, the latter is due to the oxidative decomposition of MPS latex spheres and some TMAOH included in the cages of zeolite FAU nanocrystals, as well as the loss of H_2O associated with the condensation of external surface silanol groups between zeolite nanocrystals. The total loss is about 67 wt%. The amount of inorganic components remaining is significantly larger than that obtained when using tetramethoxysilane (TMOS), titanium(IV) ethoxide (TET) and zirconium n-propoxide as the precursors to prepare macroporous silica, titania and zirconia.[6b]

Fig. 5 shows the XRD patterns of the calcined materials mentioned above prepared using zeolite nanocrystals of (a) LTA, (b) FAU, (c) LTL, (d) BEA, (e) MFI and (f) Si-MFI as building blocks, respectively. The patterns indicate that all the samples retain the same purity and high crystallinity as the original precursors. They also show that the calcination at 500 °C does not destroy the framework structures of the zeolite nanocrystals or their macroporous arrangement. The macro–micro bifunctional porous materials made from LTL, BEA and MFI nanocrystals are stable even at temperatures greater than 850 °C. However, such materials lost their macroporous long-range order after heating in boiling water for 0.5 hour.

Fig. 6 shows the SEM images of macro–micro bifunctional porous materials made using zeolite nanocrystals of (a) LTA, (b) MFI, (c) LTL and (d) BEA nanocrystals. The macro–micro bifunctional porous material prepared using LTA zeolite nanocrystals as building blocks (Fig. 6a) was templated using 1.1 μm MPS latex spheres, the others (Fig. 6b to 6d) were templated using 2 μm MPS latex spheres. 17–23 wt% shrinkage of all the samples occurred after calcination, based on the comparison of a large number of center-to-center distances in the close-packed MPS latex sphere arrays with the pore center-to-center distances in the calcined samples. However, the shrinkage was smaller than that obtained using metal alkoxide

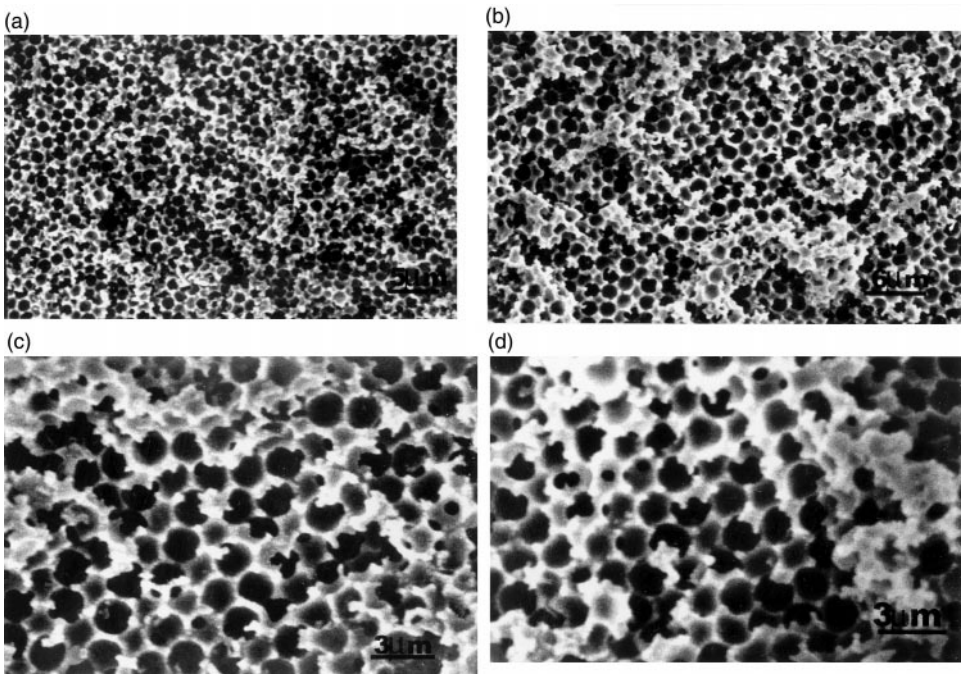

Fig. 6 SEM images of macro–micro bifunctional porous materials prepared using zeolite nanocrystals of (a) LTA, (b) MFI, (c) LTL and (d) BEA as building blocks, respectively.

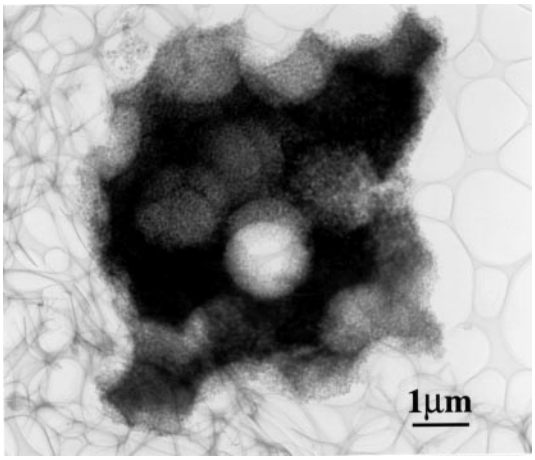

Fig. 7 A TEM image of macro–micro bifunctional porous material obtained using zeolite FAU nanocrystals as building blocks.

as precursor to prepare macroporous inorganic oxides.[6b] FT-IR spectra were used to screen the change before and after calcination. It was found that the 960 cm^{-1} bands present in as-synthesized zeolite nanocrystals, attributed to silanol groups associated with the Q^3 silicon species,[28,29] disappeared after calcination, which suggested that the shrinkage is associated with the condensation of external surface silanol groups of the zeolite nanocrystals. The periodicity of macro–micro porous material in Fig. 6b to 6d is better than that in Fig. 6a, suggesting that templates with larger sized MPS latex spheres result in more ordered macro–micro bifunctional porous materials. Fig. 6 also shows that the average wall thickness is from 150 to 190 nm, corresponding to two to three layers of nanocrystals. The walls are not uniform, the intersection between three voids is thicker than that between two voids. There are many small windows in Fig. 6d, derived from the intersection of two MPS beads, connecting the macro voids. The wall thickness also depends on the size of the MPS latex spheres. Larger sized MPS latex spheres yield thicker walled products. The SEM images indicate that macro–micro porous materials prepared from zeolite nanocrystal building blocks possess similar wall thicknesses to those reported earlier,[23,25] but much more uniform macroporous structures.

Fig. 7 shows the TEM image of macro–micro bifunctional porous material made from FAU nanocrystals. It indicates a tightly-connected FAU nanocrystal replica of close-packed MPS latex arrays. The macroporous replica structure is similar to that of macroporous alumina,[6b] however, the walls of macroporous alumina are thin (4–6 nm) and amorphous, but the walls of macro–micro bifunctional porous material made of FAU nanocrystals are thick (80–260 nm) and crystalline. The figure also shows that FAU nanocrystals are close-packed and tightly-connected.

Fig. 8 shows N_2 adsorption–desorption isotherms of macro–micro bifunctional porous materials with zeolite (a) FAU, (b) BEA and (c) MFI frameworks, respectively. The plots (Figs. 8a to 8c) exhibit a steep rise followed by flat curves at low partial pressures, indicating complete filling of the micropores with N_2. They also show quite narrow hysteretic uptakes at high partial pressures, corresponding to external micropores. The total BET surface areas were 825, 886, 790, 771, 590 and 585 $m^2\ g^{-1}$ for macro–micro porous materials with zeolite LTA, FAU, LTL, BEA, MFI and Si-MFI frameworks, respectively (Table 2). Approximately 350–660 $m^2\ g^{-1}$ of this area was due to micropores, the remainder was external to micropores. The median pore diameters were 1.072, 1.273, 0.671, 0.708, 0.619, 0.619 nm for macro–micro porous materials made of zeolite LTA, FAU, LTL, BEA, MFI and Si-MFI nanocrystals, respectively. The total single-point volumes from 0.88 to 1.03 mL g^{-1} were measured. The calculated pore volumes for pores less than 2 nm were from 0.19 to 0.29 mL g^{-1}, which indicates that the macro–micro bifunctional porous materials are composed of zeolite frameworks with almost complete crystallinity.

To prepare highly-ordered 3D macro–micro bifunctional porous materials there are several obstacles which need to be overcome: (1) preparing close-packed 3D periodic MPS latex sphere templates; (2) introducing zeolite nanocrystals to the air void systems fabricated by the MPS latex spheres; (3) finding the optimum mass ratio of zeolite nanocrystals and MPS latex spheres; (4) removing MPS templates, structure-directing molecules or H_2O without losing the long-range periodicity of the materials. There are many other techniques, such as gravity sedimentation, vertical deposition and centrifugation which allow the fabrication of highly-ordered MPS arrays. However, the next step, introducing zeolite nanocrystals to the air void system, becomes difficult, as there is no force driving the zeolite nanocrystals into the interstices between the MPS spheres. The high temperature gel conversion method, dipping centrifugated MPS templates into the reaction mixture with shaking, resulted in partially disordered MPS arrays.[23] The vacuum-assisted slow sedimentation technique, employed in this work, not only allowed the fabrication of closely-packed 3D periodic MPS latex sphere templates (Fig. 1), but also made the next step, introducing zeolite nanocrystals into the interstices between MPS latex spheres, much easier. The flowing water throughout the MPS latex arrays provides a driving force allowing the zeolite nanocrystals to permeate the interstices of the MPS latex arrays. The sizes of the zeolite nanocrystals used in this work are all limited to less than 100 nm (Fig. 2), as monitored by SEM. Such nanocrystals can be accumulated on the 0.05 μm filter membrane through the interstices between MPS latex spheres under the driving force of the flowing water. The optimum mass ratio of zeolite nanocrystals and MPS spheres was found to be about 1, under which zeolite nanocrystals permeated all the voids of MPS latex sphere templates without forming a crust on top of the samples

Table 2 Wall components, surface areas and porosity data for macro–micro bifunctional porous materials with zeolite LTA, FAU, LTL, BEA, MFI and Si-MFI nanocrystalline frameworks, respectively

Wall components	Crystallinity[a]	Total surface area/$m^2\ g^{-1}$[b]	Total pore volume/mL g^{-1}[c]	Mirpore area/$m^2\ g^{-1}$[d]	Micropore volume/mL g^{-1}[d]	Average wall thickness/nm[e]
LTA	~99	820	0.98	610	0.20	160
FAU	~99	886	1.03	660	0.23	170
LTL	~99	790	0.95	590	0.22	180
BEA	~98	771	0.94	630	0.23	180
MFI	~99	590	0.89	355	0.20	170
Si-MFI	~98	585	0.88	349	0.19	170

[a]Analysis by TEM. [b]BET surface areas. [c]Single point total pore volume of pores less than 500 nm at $P/P_o = 0.994$. [d]Calculated from a *t*-plot and MP analysis less than 2 nm. [e]Wall thickness determined by FE-SEM.

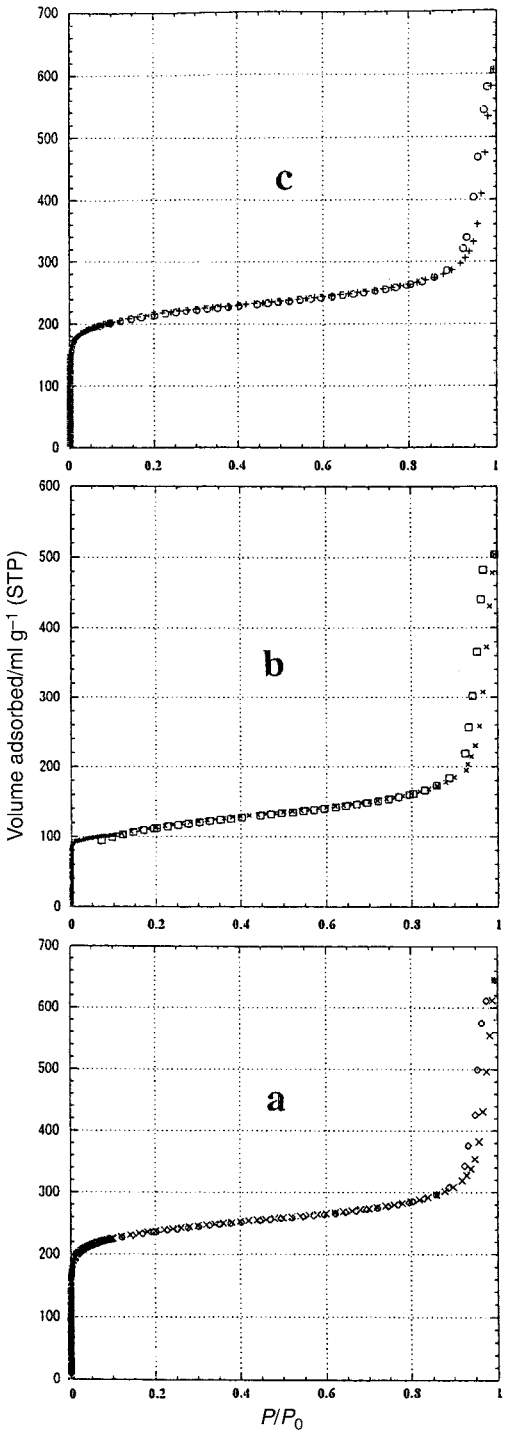

Fig. 8 N_2 adsorption–desorption isotherms of macro–micro bifunctional porous materials with zeolite (a) FAU, (b) BEA and (c) MFI nanocrystal frameworks, respectively.

(Fig. 3). In order to obtain long-range periodic macro–micro bifunctional porous materials, the low speed and two step calcination was employed to remove MPS latex sphere templates, structure-directing molecules or H_2O.

The macro–micro bifunctional porous materials obtained in this work are crack-free and self-supporting, with periodic order extending over areas of up to a centimeter. The thickness of samples can be changed from several to hundreds of microns by changing the mass of the MPS templates and zeolite nanocrystals. The macropore size can be adjusted from 1 to 11.5 μm by tuning the size of the MPS spheres. The average wall thickness between macropores is from 80 to 350 nm. The technical stability of the materials reported in this work was not measured.

Conclusion

Macro–micro bifunctional porous materials made of zeolite nanocrystals were obtained by using highly-ordered MPS latex arrays as templates, followed by calcination. The periodicity of the macro-void in the materials was predetermined by the quality and periodicity of the MPS templates. A vacuum-assisted slow sedimentation technique was employed to grow highly ordered close-packed MPS latex arrays. The void periodicity also depends on the size of both the MPS latex spheres and the zeolite nanocrystals, 2 μm MPS latex sphere arrays generate about 300 nm openings between latex spheres allowing less than 100 nm zeolite crystals to permeate the void systems smoothly. The periodic macropores of about 1–2 μm in diameter of the macro–micro bifunctional porous materials provide easier transport spaces for guest molecules. The zeolite nanocrystal frameworks with 80–350 nm thickness supply shorter diffusion paths. It was suggested that such macro–micro bifunctional porous materials would lead to zeolites with high separation and catalytic efficiencies. Analysis of the catalytic reactivity is underway.

Acknowledgements

This work was supported by CREST, Japan Science and Technology Corporation (JST), National Natural Science Foundation of China (Grant no. 29873017) and the State Basic Research Project (G2000077507). We thank Mr Weijie Jing for TG/DTA analysis, Mr Yongcun Zou for N_2 adsorption–desorption measurements, Ms Hong Ding for IR and ICP analysis and Dr Y. Sakamoto for TEM analysis.

References

1 P. Piperanski, *Contemp. Phys.*, 1983, **24**, 25.
2 H. Miguez, F. Meseguer, C. Lopez, A. Blanco, J. S. Moya, J. Requena, A. Mifsud and V. Fornes, *Adv. Mater.*, 1998, **10**, 480.
3 K. E. Davis, W. B. Russel and W. J. Glantschnig, *J. Chem. Soc., Faraday Trans.*, 1991, **87**, 411.
4 R. Mayoral, J. Requena, J. S. Moya, C. Lopez, A. Cintas, H. Miguez, F. Meseguer, L. Vazquez, M. Holgdo and A. Blanco, *Adv. Mater.*, 1997, **9**, 257.
5 P. Jiang, J. F. Bertone, K. S. Hwang and V. L. Colvin, *Chem. Mater.*, 1999, **11**, 2132.
6 (*a*) B. T. Holland, C. F. Blanford and A. Stein, *Science*, 1998, **281**, 538; (*b*) B. T. Holland, C. F. Blanford, T. Do and A. Stein, *Chem. Mater.*, 1999, **11**, 795.
7 (*a*) S. H. Park and Y. Xia, *Chem. Mater.*, 1998, **10**, 1745; (*b*) S. H. Park, D. Qin and Y. Xia, *Adv. Mater.*, 1998, **10**, 1028; (*c*) S. H. Park and Y. Xia, *Langmuir.*, 1999, **15**, 266.
8 M. Antonietti, B. Berton, C. Goltner and H. P. Hentze, *Adv. Mater.*, 1998, **10**, 154.
9 A. Imhof and D. J. Pine, *Nature*, 1997, **389**, 948.
10 A. Imhof and D. J. Pine, *Adv. Mater.*, 1998, **10**, 697.
11 J. E. G. J. Wijnhoven and W. L. Vos, *Science*, 1998, **281**, 802.
12 (*a*) S. H. Park and Y. Xia, *Adv. Mater.*, 1998, **10**, 1045; (*b*) A. A. Zakhidov, R. H. Baughman, Z. Iqbal, C. Cui, I. Khayrullin, S. O. Dantas, J. Marti and V. G. Ralchenko, *Science*, 1998, **282**, 897; (*c*) S. A. Johnson, P. J. Olliver and T. E. Mallouk, *Science*, 1999, **283**, 963.
13 (*a*) P. Jiang, J. Cizeron, J. F. Bertone and V. L. Colvin, *J. Am. Chem. Soc.*, 1999, **121**, 7957; (*b*) O. D. Velev, P. M. Tessier, A. M. Lenhoff and E. W. Kaler, *Nature*, 1999, **401**, 548; (*c*) H. Yan, C. F. Blanford, B. T. Holland, M. Parent, W. H. Smyrl and A. Stein, *Adv. Mater.*, 1999, **11**, 1003.
14 A. A. Zakhidov, R. H. Baughman, Z. Iqbal, C. Cui, I. Khayrullin, S. O. Dantas, J. Marti and V. G. Ralchenko, *Science*, 1998, **282**, 897.
15 D. W. Breck, *Zeolite Molecular Sieves*, John Wiley & Sons, New York, 1974.
16 (*a*) S. Qiu, J. Yu, G. Zhu, O. Terasaki, Y. Nozue, W. Pang and R. Xu, *Microporous Mesoporous Mater.*, 1998, **21**, 245; (*b*) G. Zhu, S. Qiu. J. Yu, F. Gao, F. Xiao, R. Xu, T. Sakamoto and O. Terasaki, *Proceedings of the 12th international zeolite*

conference, M. M. J. Treacy, B. K. Marcus, M. E. Bisher, J. B. Higgins, eds., Materials Research Society, Baltimore, 1998, pp. 1863–1870.
17 X. Meng, Y. Zhang, C. Meng and W. Pang, *Proceedings of the 9th International Zeolite Conference*, R. von Ballmoos, J. B. Higgins, M. M. J. Treacy, eds., Butterworth-Heinemann, 1992, pp. 297–304.
18 G. Zhu, S. Qiu, J. Yu, Y. Sakamoto, F. Xiao, R. Xu and O. Terasaki, *Chem. Mater.*, 1998, **10**, 1483.
19 (*a*) M. A. Camblor and J. Perez-Pariente, *Zeolites*, 1991, **11**, 202; (*b*) M. A. Camblor, A. Corma, A. Mifsud, J. Perez-Pariente, S. Valencia, *Progress in Zeolite and Microporous Materials*, H. Chon, S. K. Ihm and Y. S. Uh, eds., Elsevier, 1996, vol. 105, pp. 341–348.
20 B. J. Schoeman, J. Sterte and J. E. Otterstedt, *J. Colloid Interface Sci.*, 1995, **170**, 449.
21 B. J. Schoeman, J. Sterte and J. E. Otterstedt, *Zeolites*, 1994, **14**, 208.
22 A. E. Persson, B. J. Schoeman, J. Sterte and J. E. Otterstedt, *Zeolites*, 1994, **14**, 557.
23 B. T. Holland, L. Abrams and A. Stein, *J. Am. Chem. Soc.*, 1999, **121**, 4308.
24 (*a*) C. Madsen and C. J. H. Jacobsen, *Chem. Commun.*, 1999, 673; (*b*) I. Schmidt, C. Madsen and C. J. H. Jacobsen, *Inorg. Chem.*, 2000, **39**, 2279; (*c*) C. J. Jacobsen, C. Madsen, J. Houzvicka, I. Schmidt and A. Carlsson, *J. Am. Chem. Soc.*, 2000, **122**, 7116.
25 L. Huang, Z. Wang, J. Sun, L. Miao, Q. Li, Y. Yan and D. Zhao, *J. Am. Chem. Soc.*, 2000, **122**, 3530.
26 A. van Blaaderen, R. Ruel and P. Wiltzius, *Nature*, 1997, **385**, 321.
27 (*a*) L. V. Woodcock, *Nature*, 1997, **385**, 141; (*b*) A. D. Bruce, N. B. Wilding and G. Ackland, *J. Phys. Rev. Lett.*, 1997, **79**, 3002.
28 A. Zecchina, S. Bordiga, G. Spoto, G. Marchese, G. Petrini, G. Leofanti and M. Padovan, *J. Phys. Chem.*, 1992, **96**, 4985.
29 D. Scarano, A. Zecchina, S. Bordiga, F. Geobaldo, G. Spoto, G. Petrini, M. Padovan and G. Tozzola, *J. Chem. Soc., Faraday Trans.*, 1993, **89**, 4123.